

# Investigations into laser edge isolation (LEI) of mc-Si solar cells using ns- and ps-laser radiation

Viktor Schütz, Alexander Horn & Uwe Stute, Laser Zentrum Hannover (LZH), Hannover, Germany

- Fab & Facilities
- Materials
- Cell Processing
- Thin Film
- PV Modules
- Power Generation
- Market Watch

## ABSTRACT

In the photovoltaic industry, laser edge isolation (LEI) is a well-established process at the end of the process chain. However, because the cell properties vary from one cell producer to the next, no systematic approach is defined in industry for establishing an efficient isolation groove. Nevertheless, a general approach has to be defined for analyzing the LEI process for silicon solar cells. Besides the material aspects and laser parameters, atmospheric boundary conditions must be considered. This paper presents investigations into the ablation of a specific type of mc-silicon solar cell, and the most suitable laser, as well as the ambient parameters, is determined based on the results of the experiments.

## Introduction

Lasers are currently used within the photovoltaic industry for edge isolation, and for marking and cutting silicon solar cells. In the case of edge isolation, the  $n^+$ -doped surface layer has to be removed to guarantee the isolation of the pn-junction. The laser edge isolation (LEI) process is applicable for mc-Si solar cells using different types of laser sources. To increase the efficiency of a crystalline solar cell, high shunt resistances are necessary, and damage within the irradiated areas must be avoided. A set of laser parameters – such as wavelength  $\lambda$ , pulse duration  $t_p$  and laser fluence  $H_p$  – have already been investigated for LEI processes [1–6], with wavelengths ranging from near-infrared (NIR) to ultraviolet (UV) and pulse durations from a few picoseconds to several hundred nanoseconds. Damage can occur in the heat-affected zone during laser irradiation [7,8] and reduces the efficiency of the cell.

In order to separate the pn-junction and increase the shunt resistance to a maximum value, a theoretical minimum ablation depth of  $0.5\mu\text{m}$  is derived from the  $n^+$ -doped diffusion profile. Therefore a large absorption coefficient for ablation is required, and suitable laser sources, such as UV-lasers [9,10], must be used. In addition to wavelength, ablation for laser edge isolation depends on  $t_p$  and repetition rate  $f_{\text{rep}}$ , and results in heat load of the material. The heat penetration depth is an approximate measure of the penetration of the heat load, and possibly induces laser damage of a thin layer. The potential of selected laser sources for use in laser edge isolation will be demonstrated using distinct laser parameters.

The LEI process for silicon solar cells cannot be completely described by the laser parameters – an additional investigation of the dependence on

the process gas is necessary. The main additional process parameter is the concentration of oxygen in the process atmosphere [11]. Thus the quality of the edge isolation is highly dependent on the concentration of oxygen within the irradiated area.

## Experimental

### Solar cell specifics

Standard industrial-type isotextured mc-Si solar cells of dimension  $156 \times 156 \times 0.18\text{mm}^3$  and featuring double-side diffusion and screen-printed metallization (Fig. 1) were laser edge isolated on the front side by applying laser radiation from different sources. In the case of picosecond laser radiation, process atmospheres were also tested for their suitability in laser edge isolation.

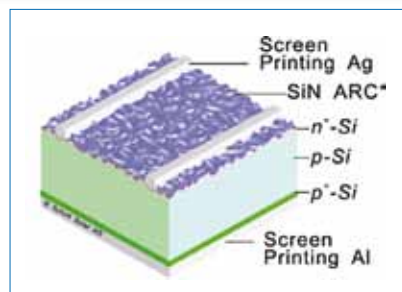


Figure 1. Structure of a mc-Si solar cell with an  $n^+$ -doped surface layer.

The ablation depth required for effective laser edge isolation can be derived from the  $n^+$  (phosphor) dopant concentration distribution. In the case of the investigated solar cells, the dopant concentration decreases to the ground-doped level at a depth of approximately  $0.5\mu\text{m}$ , and corresponds to the minimum

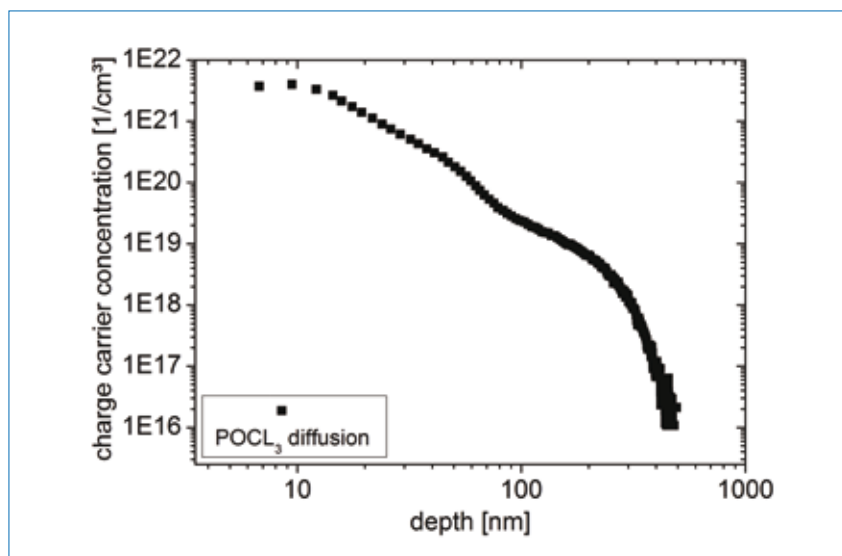


Figure 2.  $n^+$ -dopant (phosphor) concentration of mc-Si solar cells versus depth (data from Schott Solar AG), showing the ground-doped level at a charge carrier concentration of approximately  $10^{16}\text{cm}^{-3}$ .

required ablation depth at a charge carrier concentration of approximately  $10^{16}\text{cm}^{-3}$  – the so-called ‘ground-doped level’ (Fig. 2).

A typical dopant concentration profile of phosphorous in silicon depends on two diffusion mechanisms during production, which are dominant at different charge carrier concentrations and diffusion velocities. The highly doped regime is dominated by vacancy diffusion, whereas the poorly doped regime is dominated by interstitial diffusion. The well-known kink-and-tail carrier distribution results because of the different diffusion mechanisms of phosphor in silicon [12]. The charge carrier concentration converges asymptotically towards the ground-doped level [13].

“The parallel resistance of a silicon solar cell depends on the dopant profile and the corresponding specific resistivity at this charge carrier concentration.”

The parallel resistance of a silicon solar cell depends on the dopant profile and the corresponding specific resistivity at this charge carrier concentration. Both these dependencies have to be related in order to determine the correlation between the shunt resistance and the ablation groove depth. Therefore the  $n^+$ -dopant concentration as a function of depth is the crucial parameter and determines the ablation depth for sufficient laser edge isolation. The specific resistivity  $\rho$  of phosphorous-doped silicon depends on the charge carrier concentration  $A$ , and the achievable shunt resistances can be estimated at a certain groove depth by plotting  $A$  versus  $\rho$  (Fig. 3). The dependence of the specific resistivity on the charge carrier concentration can potentially be described by the expression

$$\rho(A) = a \cdot A^b \quad (1)$$

where  $a$  and  $b$  are numerical fit parameters. The  $A$ - $\rho$  dependence, taken from Beadle et al. [14], is fitted in three regimes shown in Fig. 3, and the fit parameters for the three regimes are listed in Table 1.

Regime	$a$ [ $\Omega\cdot\text{cm}^4$ ]	$b$
1	1015	-0.9549
2	568.25	-0.2253
3	1014	-0.8599

Table 1. Fit parameters for the three regimes in Fig. 3.

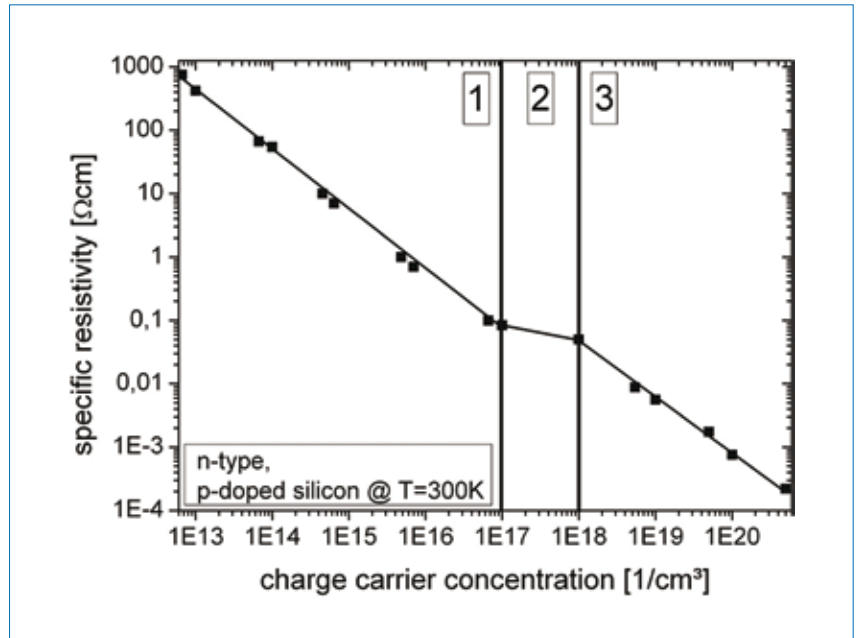


Figure 3. Specific resistivity of n-type phosphorous-doped silicon at room temperature versus charge carrier concentration (data taken from Beadle et al. [14]).

From Figs. 2 and 3, the dependence of specific resistivity  $\rho(z)$  on depth can be derived as shown in Fig. 4.

#### Laser set-up specifics and parameters

The laser edge isolation process was investigated by applying ns- and ps-laser radiation to mc-Si solar cells. The cells were processed at identical ambient conditions to allow an evaluation of shunt resistance as a function of laser ablation depth to be made.

Laser scanners were used to position the focused laser radiation along the desired path. For the investigations, optics with focal lengths of 255mm and 250mm were used. The relevant parameters for different laser systems are

listed in Table 2. Different groove depths were generated by laser ablation using the laser sources indicated in the table. The groove depth was measured by optical microscopy, and the corresponding shunt resistance was determined by dark I-V measurements.

In addition, several gases were tested (at 1 bar at room temperature in normal ambient atmosphere, oxygen, nitrogen and argon) for their suitability as processing atmospheres in the laser edge isolation process. These experiments were carried out with Laser 1, and three characteristic laser parameter sets were tested for edge isolation. The structural and chemical investigations of the laser grooves were conducted using scanning electron

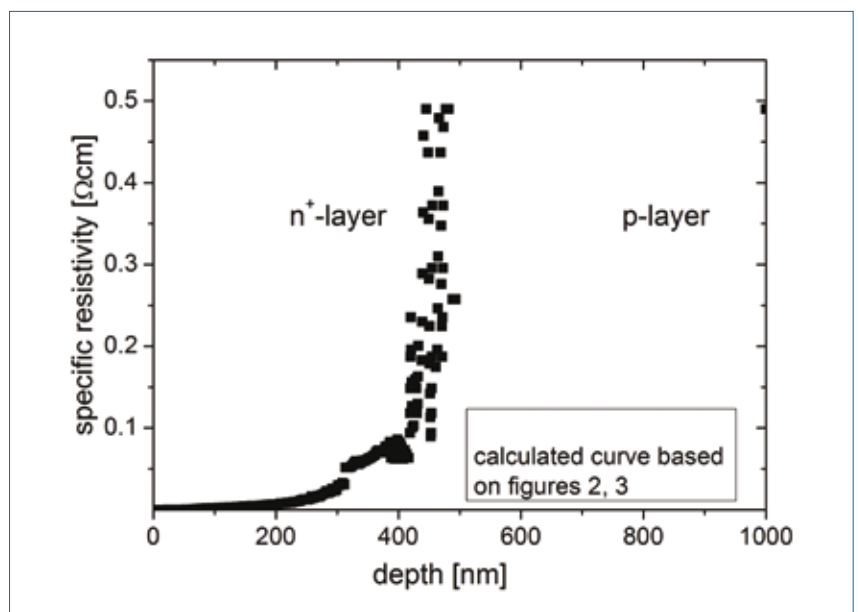


Figure 4. Specific resistivity of n-type phosphorous-doped silicon at room temperature versus depth, based on Figs. 2 and 3.

	Laser	$\lambda$ [nm]	$t_p$ [ns]	$H_{p,max}$ [J/cm <sup>2</sup> ]	$f_{rep}$ [kHz]	$f_{foc}$ [mm]
1	Trumpf: TruMicro 5X50 2 $\omega$	515	0.007	14	400	255
2	Trumpf: TruMicro 5X50	1030	0.007	6.2	400	255
3	Rofin: RSM E20	532	7	21.7	15	250
4	Rofin: RSM E20	532	13	14.4	40	250
5	IPG: YLPM-1-A4-20-20	1064	20	7.6	100	255
6	IPG: YLP-1-120-50-50	1064	120	31.3	50	255

Table 2. Laser systems and relevant laser parameters.

microscopy (SEM) and energy dispersive X-ray spectroscopy (EDX).

### Characteristics of the laser edge isolation process

A small specific resistivity – the initial potential – at the top of the solar cell can be identified. With increasing depth the specific resistivity increases to its maximum – the capacity limit (Fig. 4). The resistivity is then determined from the specific resistivity, using the general equation

$$R_{sh}(z) = \rho(z) \cdot \frac{A(z)}{L} \quad (2)$$

where  $R_{sh}$  represents the resistivity,  $\rho(z)$  is the depth-dependent specific resistivity,  $L$  is the length of the edge of the solar cell, and  $A(z)$  is the product of the groove width

( $d_{gr}$ ) and residual thickness (difference of the thickness  $z$  of the solar cell and the ablation groove  $a$ ).

“With increasing depth the specific resistivity increases to its maximum.”

The variation of  $R_{sh}$  as a function of groove depth can be mathematically described using an empirically derived logistic growth approach. This type of growth is best described by the differential equation [15]

$$\frac{dR_{sh}(z)}{dz} = k \cdot R_{sh}(z) \cdot (R_{sh,max} - R_{sh}(z)) \quad (3)$$

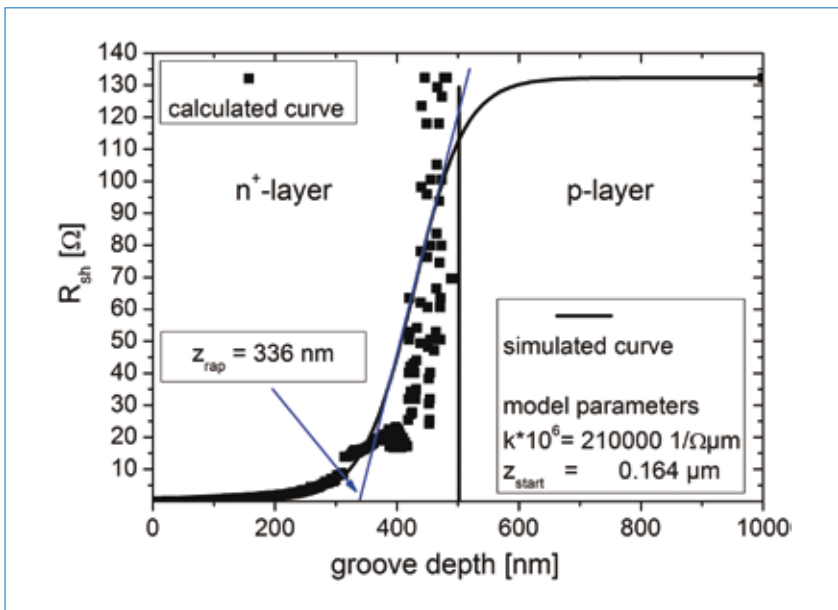


Figure 6. Resistivity as a function of groove depth, determined from Figs. 2 and 3 and modelled using Equation 4 (edge length of the solar cell  $L = 156$ mm; area of laser beam diameter and solar cell thickness  $A = 4212\mu\text{m}^2$ ).

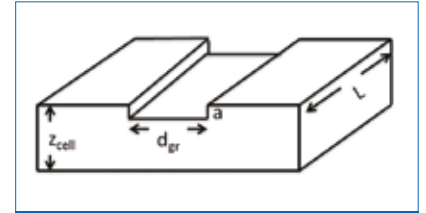


Figure 5. Schematic of the laser-generated groove for evaluating Equation 2.

where the parameter  $R_{sh,max}$  represents the shunt resistance capacity limit of the solar cells, and the logistic parameter  $k$  is a measure of the change of the groove depth-dependent shunt resistance. A solution of the differential equation is given by

$$R_{sh} = R_{sh,max} \cdot \frac{1}{1 + \exp[-k \cdot R_{sh,max} \cdot (z + z_{start}) \cdot (\frac{R_{sh,max}}{R_{sh,N=0}} - 1)]} \quad (4)$$

where  $R_{sh,N=0}$  represents the initial shunt resistance,  $z$  the depth and  $z_{start}$  the depth value at which the shunt resistance starts to increase with depth (and therefore depends on the underlying dopant profile). Another, more convenient, value for determining the rapid start of growth of the shunt resistance with depth is defined by  $z_{rap}$ , and will be used to empirically determine the carry-over of the dopant profile. The intersection of the tangent of the model curve of Equation 4 at the turning point with the abscissa defines  $z_{rap}$ , and is given by the equation

$$z_{rap} = \frac{\ln[\frac{R_{sh,max}}{R_{sh,N=0}} - 1] - R_{sh,max} \cdot k \cdot z_{start} - 2}{R_{sh,max} \cdot k} \quad (5)$$

Based on the described model, the data taken from Fig. 4 and Equation 2 can now be modelled using Equation 4. This is an idealized graph of shunt resistance versus groove depth. The minimum charge carrier concentration is taken as a reference for the ground-doped level as it is not measured (Fig. 2). The ideal case defined by the dopant profile in Fig. 2 is  $z_{rap,ideal} = 336$ nm and shown in Fig. 6.

The efficiency of the laser edge isolation process in terms of ablation depth required to reach the intersection of the tangent and the abscissa is then defined as

$$\eta = \frac{z_{rap,ideal}}{z_{rap,laser}} \cdot 100\% \quad (6)$$

In order to compare the results with different repetition rates, the normalized laser edge isolation efficiency  $\eta_{norm}$  is introduced and defined through a normalized  $z_{rap,laser,norm}$  as

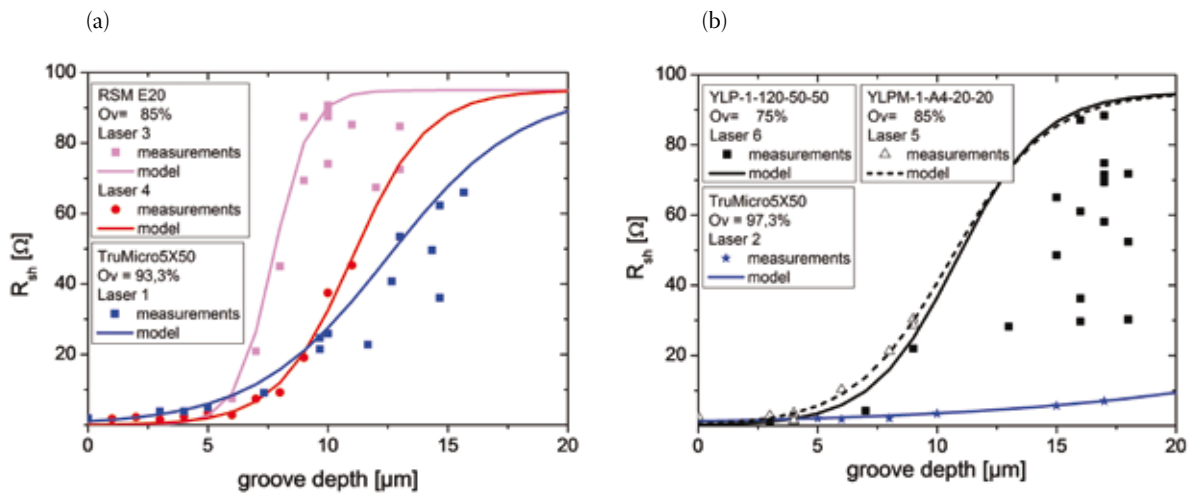


Figure 7. Shunt resistance versus groove depth for various laser systems and modelled logistic functions.

$$\eta_{norm} = \frac{z_{rap,ideal}}{z_{rap,laser,norm}} \cdot 100\% \tag{7a}$$

$$z_{rap,laser,norm} = \frac{z_{rap,laser}}{N_{ppp}} \tag{7b}$$

$$N_{ppp} = \frac{d_{gr} \cdot f_{rep}}{v} \tag{7c}$$

where the parameter  $N_{ppp}$  is the number of laser pulses per point.

### Results and discussion

#### Shunt resistance as a function of laser-ablated groove depth

The shunt resistance as a function of groove depth was determined for five laser systems, and different laser pulse durations, wavelengths and repetition rates were investigated. The measured shunt

resistances were fitted to the developed logistic model (Equation 4); also, the relevant model parameters, specifically  $k$  and  $z_{rap}$ , were determined to estimate the efficiency of the laser edge isolation process. The limitations of these laser systems can be determined by plotting the logistic model curve against groove depth per pulse. By doing this, it is possible to determine the most feasible laser parameters that will minimize damage to the solar cell in the laser edge isolation process. The relevant derived model parameters are

THE  
WET PROCESSING  
COMPANY

R | E | N | A | ●



## New RENA WaSep unit separates 3,000 - 6,000 wafers/hour

The latest generation RENA WaSep separates up to 6,000 wafers/h (double unit) with a breakage rate < 0.5%. The world's only production proven wet wafer separation system.

More at [www.rena.com](http://www.rena.com)



Laser	$z_{rap,laser}$ [ $\mu\text{m}$ ]	$z_{rap,laser,norm}$ [ $\mu\text{m}$ ]	$\eta$ [%]	$\eta_{norm}$ [%]
1	6.9	0.490	4.9	68.6
2	20.4	0.503	1.7	66.8
3	6.2	0.897	5.4	37.5
4	7.5	1.160	4.5	30.0
5	6.5	0.963	5.2	34.9
6	9.0	1.877	3.7	17.9

Table 3. Relevant model parameters for different laser systems and corresponding laser edge isolation efficiencies ( $z_{rap,ideal} = 0.336\mu\text{m}$ ).

$z_{rap,laser}$ ,  $z_{rap,laser,norm}$  and  $z_{rap,ideal}$  (see Table 3), and accordingly the laser edge isolation efficiencies  $\eta$  and  $\eta_{norm}$  can be determined.

The differences between the theoretical predicted groove depth of  $0.5\mu\text{m}$  for complete edge isolation and the values obtained experimentally can be explained by thermodynamic assumptions and, to a lesser extent, by impurities, redeposition of particles, surface topology and a non-ideal behaviour of mc-Si solar cells.

In the first step, the laser radiation is partially absorbed by the silicon. The optical energy is transformed into phonon energy, e.g. oscillation energy of atoms of the compound, which is, from a macroscopic perspective, a heat load. The

heat dissipates afterwards by diffusion. The laser energy in the material accumulates by consecutive laser irradiations, until energy input and energy losses equalize. However, the temperature of the material rises steadily as a consequence of energy accumulation, thus producing diffusion of the dopants into the bulk material according to Fick's laws. The diffusion constant of phosphor in silicon rapidly increases with rising temperature [16]. With a series of large energy laser radiation pulses, a surface temperature close to the melting point of silicon is reached in a timescale of tens of microseconds. At this diffusion time, the diffusion length is of the order of several micrometres, based

on equations in [16]. As a consequence, the model parameters  $k$ ,  $R_{sh,max}$  and  $z_{start}$  are also functions of the thermodynamic properties of silicon.

The statistical spreading of the measured shunt resistances at certain groove depths is due to local shunts in the cell area, which result in a decrease in  $R_{sh}$ . Nevertheless, with the laser parameters used, the logistic curve (Equation 4) satisfactorily describes the maximum achievable shunt resistances as a function of depth. In all cases, improvements are possible whereby the energy losses due to heat dissipation are reduced. Shorter pulse durations and shorter wavelengths, resulting in a smaller ablation rate, are preferable for the edge isolation process: first, there is less heat load and a smaller heat-affected zone; and second, there is a larger absorption of laser radiation. By using wavelengths and pulse durations that ensure a heat-affected zone in the region of  $z_{rap,ideal}$ , a saving of laser power is indicated for the laser edge isolation process. With a smaller  $z_{rap,laser}$  (see Table 3), less carry-over of the dopants is induced by the solar cell and therefore higher maximum laser edge isolation efficiencies are achievable.

“Shorter pulse durations and shorter wavelengths, resulting in a smaller ablation rate, are preferable for the edge isolation process.”

Solar cells could not be isolated by a  $500\text{nm}$  deep groove using laser radiation with a laser wavelength of  $\lambda = 515/1030\text{nm}$ ; even with ultra-short laser pulses in the optical ablation regime [5,6,15], for which the heat load is minimal, it still was not possible. The ablation rate for laser radiation with a pulse duration of  $t_p = 7\text{ps}$  in the optical ablation regime of silicon is smaller than  $200\text{nm}$ . As a result, additional laser pulses are required to remove the  $n^+$ -layer completely, leading to a thermal load of the silicon and diffusion of the dopants. In consequence, ns-laser pulses are preferable in the case of pulse energies which support an effective melt ejection and because of their larger thermal penetration depth of approximately  $d_{th} = 1\mu\text{m}$ , occurring at a pulse duration of  $t_p = 7\text{ns}$  at  $T = 300\text{K}$ . This corresponds to a value that is at least twice as large as the doped depth, and is therefore, in a first approximation, sufficient for removing the  $n^+$ -layer with a limited amount of laser pulses.

Shunt resistance as a function of different ambient gases and topologies

Different characteristic laser processing parameter sets ( $H_p$ ,  $O_v$ ) were used for the laser edge isolation with different ambient

$H_p$ [ $\text{J}/\text{cm}^2$ ]	14	1	1
$O_v$ [%]	93.33	99.63	99.91
$\text{O}_2$			
Ambient atmosphere			
$\text{N}_2$			
Ar			

Table 4. Different groove types generated in an ambient atmosphere,  $\text{O}_2$ ,  $\text{N}_2$  and Ar for three characteristic laser parameters (where  $f_{rep} = 400\text{kHz}$ ,  $d_f = 23.4\mu\text{m}$  and  $O_{rest}$  is the remaining atomic oxygen concentration in the laser groove).

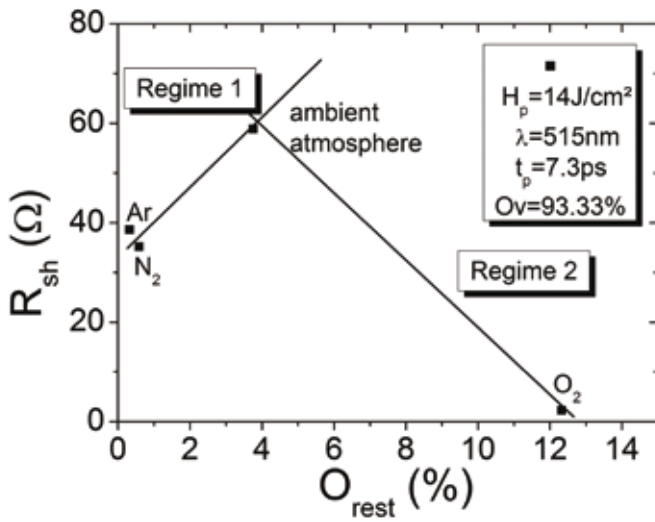


Figure 8. Shunt resistance as a function of remaining oxygen concentration  $O_{rest}$ .

gases. With these parameter settings, three groove structure types are distinguished.

Generation of grooves by laser ablation with a fluence of  $H_p = 14 \text{ J/cm}^2$  and an overlap of  $Ov = 93.33\%$  results in typical v-shaped groove geometries as shown in Table 4. However, the measured groove depths of approximately  $15 \mu\text{m}$  at  $H_p = 14 \text{ J/cm}^2$  do not depend on the investigated atmospheres. At a fluence of  $H_p = 1 \text{ J/cm}^2$  and overlaps of  $Ov = 99.63\%$  and

$Ov = 99.91\%$ , a cone-like structure and a deep, narrow groove are generated respectively [11]. The characteristic geometrical structures at  $H_p = 1 \text{ J/cm}^2$  and different overlaps do not depend on the process gas type and the geometry does not change. The main observed differences are electrical and chemical in nature. The shunt resistances and the remaining oxygen concentration in the groove vary over a wide range for different laser parameters and gases (Table 4).

As seen in Table 4, laser processing in argon and nitrogen atmospheres results in smaller shunt resistances. In the case of industrially-relevant laser parameters, such as velocity ( $v \geq 0.624 \text{ m/s}$ ), the most suitable process gas is in fact ambient atmosphere. Increasing the oxygen content causes, at a scanning velocity of  $v = 0.624 \text{ m/s}$  (corresponding to  $Ov = 93.33\%$ ), a reduction of the shunt resistance of the solar cells. Edge isolation in the optical regime and at a smaller scanning velocity (and therefore at larger overlaps) yields larger shunt resistances, but isolating with these parameters corresponds to an insufficient throughput. Increasing the remaining oxygen concentration increases the shunt resistance to a maximum; a further increase of the oxygen concentration then causes the shunt resistance to decrease significantly (Fig. 8).

The increase of the shunt resistance due to a larger oxygen concentration (regime 1 in Fig. 8) is possibly due to passivation of the ablation edges after irradiation; on the other hand, the decrease of the shunt resistance with further increase in oxygen concentration (regime 2 in Fig. 8) can be explained by diffusion of impurities. This is based on the different characteristic process timescales for the passivation and diffusion during laser edge isolation. Secondary ion mass spectroscopy (SIMS) measurement of the tentative dopant profile in the laser-

## UPGRADE CELL PERFORMANCE BY BACK SIDE PASSIVATION WITH $\text{Al}_2\text{O}_3$

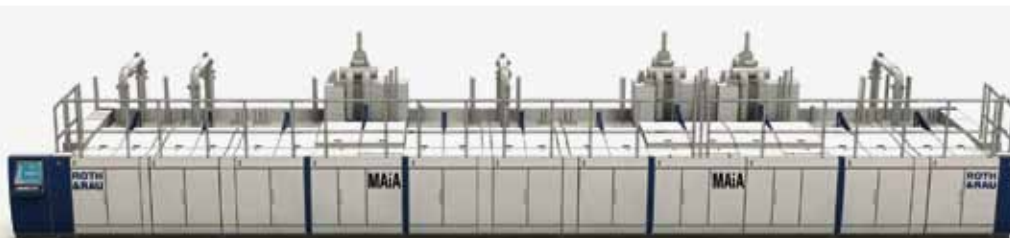
Aluminium oxide ( $\text{Al}_2\text{O}_3$ ) has been found as an excellent means for the passivation of the wafer backside. Thus, the passivation of the wafer backside leads to a considerable improvement of the cell efficiency – up to 19% and more. Basing on the industrially proven anti-reflection coating equipment  $\text{SiNA}^\circ$ , the  $\text{MAiA}^\circ$  system has been developed to provide a double side coating tool for solar cells, in which all coating steps for back side passivation plus the anti-reflection coating of the front side can be carried out in one run.

### 3 PROCESS STEPS – 2 SIDES – 1 SYSTEM ONLY



**ROTH & RAU**

Roth & Rau AG  
An der Baumschule 6-8  
09337 Hohenstein-Ernstthal  
Germany  
Phone +49 (0) 3723 - 66 85 - 0  
Fax +49 (0) 3723 - 671 - 1000  
E-mail [info@roth-rau.com](mailto:info@roth-rau.com)  
[www.roth-rau.com](http://www.roth-rau.com)



ablated grooves (which are necessary for edge isolation) failed due to the roughness of the bottom of the groove. To evaluate these proposed mechanisms, passivation and diffusion, other characterization tools need to be used.

## Conclusion

The shunt resistance of mc-Si solar cells after laser edge isolation is characterized by three process mechanisms, each with a different emphasis. In general the value of the shunt resistance is a function of the three process mechanisms: ablation depth, passivation of ablation edges and diffusion of impurities.

In the case of depth-dependent shunt resistance, a logistic model approach has been derived which satisfactorily describes the shunt resistance as a function of ablation depth. In the other two cases – passivation and diffusion – preliminary results have been presented. Based on these empirical investigations and the developed logistic model, it is possible to determine optimal laser parameters for laser edge isolation at a specific charge carrier distribution. The dominant process during laser edge isolation depends on the three characteristic process times for heat diffusion, phosphor diffusion and passivation.

**“The best-suited atmosphere is standard ambient atmosphere.”**

A theoretical representative set of efficient laser parameters for achieving higher solar cell efficiencies is given for a certain optical set-up. A typical optical set-up is equipped with an f-theta lens with a focal length of  $z_{\text{lens}} = 292\text{mm}$  and a collimated raw beam diameter of  $d_{\text{raw}} = 5.5\text{mm}$  at  $1/e^2$ . Complementing this optical set-up, the laser source should provide an output power of  $P_m \geq 23.1\text{W}$  at a repetition rate of  $f_{\text{rep}} = 30\text{kHz}$ . Furthermore, a pulse duration of  $t_p = 7\text{ns}$  at a laser wavelength of  $\lambda = 532\text{nm}$  and a beam quality factor  $M^2 < 1.5$  will be required. With these parameters it is possible to ensure a scribing velocity of  $v \geq 624\text{mm/s}$  for a 6-inch solar cell having a charge carrier concentration distribution comparable to that shown in Fig. 1. The scaling of the required laser power for sufficient edge isolation increases in a non-linear way for faster scribing velocities and larger focal diameters, and especially for higher repetition rates. Moreover, the best-suited atmosphere is standard ambient atmosphere.

## Acknowledgment

The authors would like to express their gratitude for funding provided by

the German Federal Ministry for the Environment, Nature Conservation and Nuclear Safety (BMU) under Contract No. 0325053.

## References

- [1] Emanuel, G. et al. 2001, “High throughput laser isolation of crystalline silicon solar cells”, *Proc. 17th EU PVSEC*, Munich, Germany, pp. 1578–1581.
- [2] Muellers, L. et al. 2008, “Analysis of different laser concepts for edge isolation of crystalline solar cells”, *Proc. 23rd EU PVSEC*, Valencia, Spain, pp. 1670–1672.
- [3] Kray, D. et al. 2007, “Study on the edge isolation of industrial silicon solar cells with waterjet-guided laser”, *Solar Energy Mater. & Solar Cells*, Vol. 91, No. 17, pp. 1638–1644.
- [4] Hauser, A. et al. 2001, “Comparison of different techniques for edge isolation”, *Proc. 17th EU PVSEC*, Munich, Germany, pp. 1739–1741.
- [5] Haupt, O. et al. 2009, “Improved laser edge isolation of crystalline silicon solar cells using a high power picosecond laser”, *Proc. ICALEO*, Orlando, Florida, USA.
- [6] Haupt, O. et al. 2009, “Excellent edge isolation of crystalline silicon solar cells obtained by high power picosecond laser”, *Proc. 24th EU PVSEC*, Hamburg, Germany.
- [7] Haupt, O. 2008, “Laser dicing of silicon: Comparison of ablation mechanisms with a novel technology of thermally induced stress”, *Proc. 9th Int. Symp. on Laser Prec. Microfab.*, Quebec City, Canada.
- [8] Schoonderbeek, A. et al. 2006, “Laser technology for cost reduction in silicon solar cell production”, *Proc. ICALEO*, Scottsdale, Arizona, USA.
- [9] Bäuerle, D. 2000, *Laser Processing and Chemistry*, 3rd edn. Heidelberg: Springer Verlag.
- [10] Colville, F. 2009, “Laser scribing tools edge in front”, *Global Solar Technology*, March/April, pp. 12–15.
- [11] Schütz, V. and Stute, U. 2011, “The influence of atmospheric components during laser edge isolation”, *Proc. 26th EU PVSEC*, Hamburg, Germany.
- [12] Uematsu, M. 1997, “Simulation of boron, phosphorus, and arsenic diffusion in silicon based on an integrated diffusion model, and the anomalous phosphorus diffusion mechanism”, *J. Appl. Phys.*, Vol. 82, No. 5, pp. 2228–2246.
- [13] Kränzle, A. 2007, “Industriesolarzellen auf dünnem multikristallinem Silizium: Diffusionsverfahren, neue Materialien und bifaciale Strukturen”, Dissertation, Universität Konstanz.

- [14] Beadle, W.E. et al. 1985, *Quick Reference Manual for Silicon Integrated Circuit Technology*. New York: Wiley.
- [15] Schütz, V. et al. 2010, “Laser edge isolation with a focus on damage reduction by the use of ultra-short pulse lasers”, *Proc. 25th EU PVSEC*, Valencia, Spain.
- [16] Fair, R.B. 1981, “Concentration profiles of diffuse dopants in silicon”, in Yang, F.Y., Ed., *Impurity Dopant Processes in Silicon*. Amsterdam: North Holland.

## About the Authors



**Viktor Schütz** graduated from the Photonics programme at the University of Applied Sciences Oldenburg/Ostfriesland/Wilhelmshaven in 2008. He has been working as a scientist at LZH in the field of photovoltaics, semiconductors and simulations since October 2008.



**Alexander Horn** studied physics in Siegen, Germany, and graduated in 2003. After that he became senior scientist holding the chair in Laser Technology (LLT) of the RWTH Aachen, and then leader of the Ultrafast-Technology group in 2004. In 2008 he took up a new position as a representative professor at the Institute for Physics of the University of Kassel, Germany. Dr. Horn is now the head of the Photovoltaics group at LZH, where his main field of research is the ultra-fast detection of laser-induced processes, especially the development and usage of novel pump and probe techniques. He has authored more than 56 scientific publications.



**Uwe Stute** was awarded a Ph.D. in physics in 2001. Since then he has worked on laser production technology at LZH, followed by photovoltaic applications in industry. In 2010 Dr. Stute went back to LZH as manager of the department of technologies for non-metals, which incorporates laser applications relating to glass, photovoltaic and carbon-reinforced plastics.

## Enquiries

Viktor Schütz  
Laser Zentrum Hannover e.V.  
Technologies for Non-Metals Department  
Hollerithalle 8  
30419 Hannover  
Germany  
Tel: +49 (0) 511-2788-329  
Email: v.schuetz@lzh.de